Project report for SCEC Award 19207: "Understanding the triggering process of the foreshock sequence of the 2010 M7.2 El-Mayor-Cucapah earthquake"

Abstract:

Understanding the triggering mechanism of foreshocks and their relationship to large earthquakes is very important for earthquake forecasting and hazard mitigation. Two models have been proposed to foreshocks: "pre-slip" where foreshocks are triggered by aseismic processes in the mainshock nucleation zone; "cascading failure" where foreshocks are triggered by series of cascading failure. Continuing debates are ongoing for the triggering mechanism of foreshocks. In this study, we reanalyze the foreshocks for the 2010 M7.2 El-Mayor-Cucapah earthquake using new data, improved spectral analysis method and new locations. The results from the new method show good agreement with results from spectral ratio analysis. The results show increased level of stress interaction within 0.5 km of the mainshock starting about 9 days before the mainshock, which accelerated during the last day. This suggests cascading failure during foreshocks, and between foreshocks and the mainshock. The results also show some isolated foreshocks with no stress interactions, and some foreshocks occurring within rupture zones of previous earthquakes, which suggests possible aseismic stressing process. Collectively, these observations support an alternative foreshock model: "swarmy foreshock", where the foreshock themselves are independent of the mainshock nucleation process, but the foreshocks and the possibly associate aseismic process contribute to the stress loading at the mainshock hypocenter.

Intellectual merit:

The research contributes to new understanding of the triggering process during the El-Mayor-Cucapah earthquake mainshock. The results suggest the importance of improved data recording and analysis method in understanding triggering processes. In practice, there is no clear boundary between the two end-members of foreshock triggering processes. Both aseismic slip and cascading failure can occur during foreshock sequences. The results support the alternative "swarmy foreshock" model, and highlight the importance to understand earthquake swarms in seismic hazard evaluation. In addition, comparison of source parameter estimates suggests the improved stacking method can obtain the same results for the same events from spectral ratio analysis.

Broader impacts:

The project results are beneficial for learning earthquake hazards, risks and earthquake physics. The project contributed to the training and education of students and postdocs at OU. Graduate student Jiewen Zhang adapted and refined an improved stacking algorithm, and postdoc Qimin Wu developed and refined a new time-domain deconvolution method.

Technical report:

1. Project objective:

We plan to apply a new stacking based method (Chen & Abercrombie, 2020) to new data from Mexico seismic network to analyze the triggering process of foreshocks during the 2010 M7.2 El Mayor-Cucapah earthquake. The results will be used to understand the roles

of Coulomb stress transfer in foreshock sequences and the triggering of the mainshock itself.

2. Research progress

Data and catalog

We obtain event waveforms, phase picks and relocations from Dongdong Yao (Yao, Huang, Peng, & Castro, 2020) (Figure 1). We calculate displacement spectra using multi-taper program for both P and S-waves using 2s and 3s windows following picked arrival for M<3 earthquakes. For earthquakes larger than 3, the time window extends to 4s and 6s for P and S waves. The noise window has the same length as the P-wave window and ends immediately before P-wave arrival. The time windows are longer than Chen & Shearer, (2013) and also includes S-wave. We select spectra that have signal-to-noise ratio (SNR) greater than 3 between 1 and 20 Hz, and events with at least 5 stations meeting the SNR requirement for further analysis. We use both P and S-wave spectra for the data analysis.

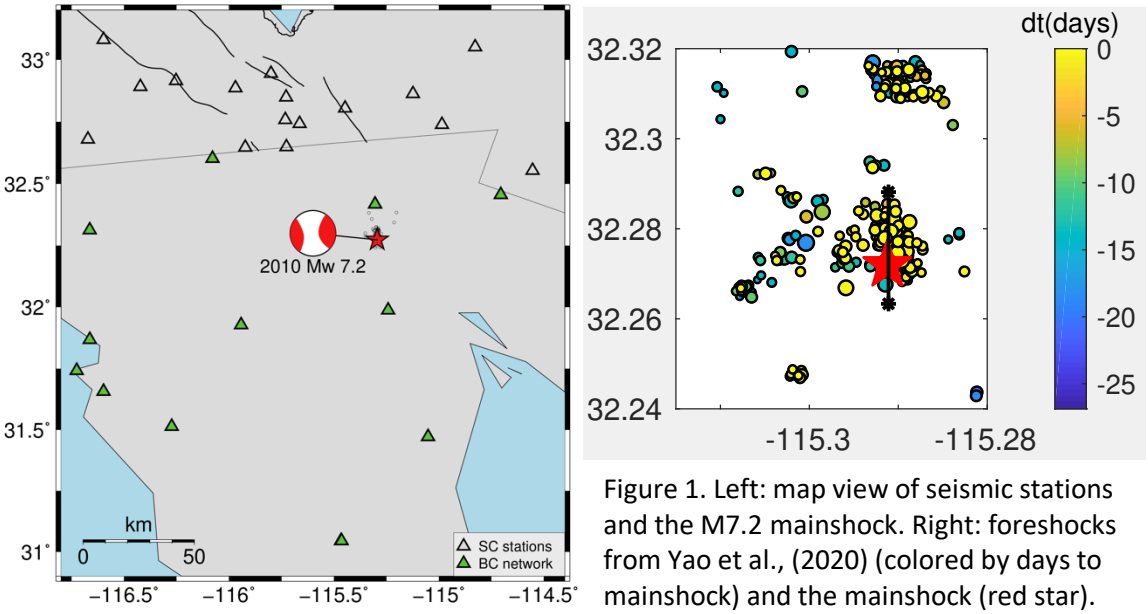

Figure 1. Left: map view of seismic stations and the M7.2 mainshock. Right: foreshocks from Yao et al., (2020) (colored by days to mainshock) and the mainshock (red star). The black line shows the NS fault line delineated by foreshocks.

Methods:

Spectral analysis:

We first apply the spectral decomposition method in Shearer et al., (2016) to isolate event term, station term and path term. Then, we perform magnitude calibration between low-frequency spectral amplitude and catalog magnitude to obtain improved moment magnitude. Next, we apply the improved stacking analysis named "SNSS" in Chen & Abercrombie (2020) to stacked event term to obtain an empirical correction spectrum (ECS). After correcting individual earthquakes with the ECS, we will fit Brune-model to obtain the best-fitting corner frequency. The major difference between "SNSS" and the method in Shearer et al., (2006) is that "SNSS" does not enforce all magnitude bins to have same stress drop ("self-similarity"). The new method is more suitable for smaller dataset when different magnitude bins can have different reference stress drops. Synthetic tests in

Chen & Abercrombie (2020) suggest that "SNSS" performs better than the previous stacking method, especially for smaller datasets that have larger standard deviation.

Model stress change:

We follow Ellsworth & Bulut (2018) and Yoon et al. (2019) to model the slip for each earthquake. We compute rupture radius based on shear wave velocity and the corner frequency: $R = \frac{kv_s}{f_c}$, where k=0.26 is the constant from Kaneko & Shearer (2014), Vs is the shear wave velocity interpolated based on 1D velocity model of southern California and relocated event depth, fc is the corner frequency of each event from spectral analysis.

We calculate the average slip on the circular fault patch: $D = \frac{M_0}{\mu\pi R^2}$, where M_0 is the seismic moment, $\mu = 30\ GPa$ is the assumed shear modulus, and R is the source radius calculated from corner frequency. The static constant stress drop is computed by assuming a circular fault patch (Eshelby, 1957): $\Delta\sigma = \frac{7M_0}{16R^3}$.

The slip within the circular rupture is modeled using this function:

$$d(r) = D\left[1 - \left(\frac{r}{R}\right)^2\right]^{\frac{3}{2}} \quad (r < R), or\ 0\ (r > R)$$

where r is the radius within the rupture.

We then digitize the fault plane into small grids (0.005 km by 0.005 km) and calculate cumulative stress changes resolved at each grid.

Results

Comparison with previous results

We first compare new results with P-wave stacking results from Chen & Shearer (2013) and spectral ratio results using S-wave from Yao et al., (2020) (Figure 2). Because all the methods use corner frequency to compute the final stress drop, we only compare corner frequencies from different studies. Overall, the S-wave results are in good agreement with Yao et al., (2020) with correlation coefficient of 0.97. The P-wave results from this study are also strongly correlated with Yao et al (2020) (correlation coefficient of 0.965), albeit with systematically lower corner frequency values, which are similar to Chen & Shearer (2013). The cause of the low corner frequency from P-wave is unclear, however, Chen & Abercrombie (2020) note that S-wave gives the most

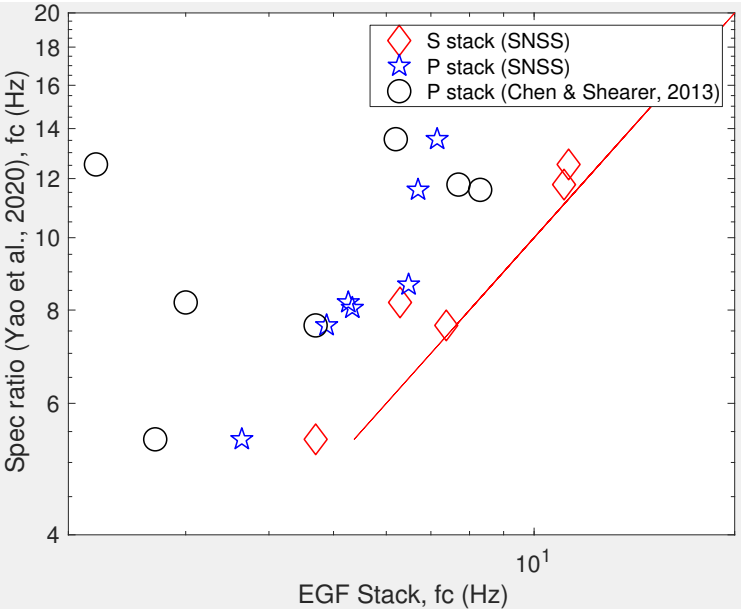

Figure 2. Comparison among different studies. The red line denoted one-to-one ratio of corner frequency. The new results with SNSS method are more correlated with each other, and with spectral ratio results from Yao et al., 2020.

consistent results with different signal-to-noise ratio criteria. Because of the agreement for S-wave from multiple methods, we chose S-wave results for the stress analysis.

Stress changes during foreshock sequence

Figure 3 shows the result of modeled stress changes from all foreshocks within 15 days of the mainshock using the location from Yao et al., (2020). Both along depth and map view of stress changes show a cascading failure bursts within 0.6 km of the mainshock. Detailed temporal evolution of foreshocks suggests that the earliest foreshocks have limited stress interactions with each other (Figure 4). The foreshock started to cluster around the mainshock at 10 and 9 days before the mainshock. The last two foreshocks within the last day occurred within tens of meters of the mainshock hypocenter. Several foreshocks have rupture areas overlapping with areas of positive stress changes from previous foreshocks.

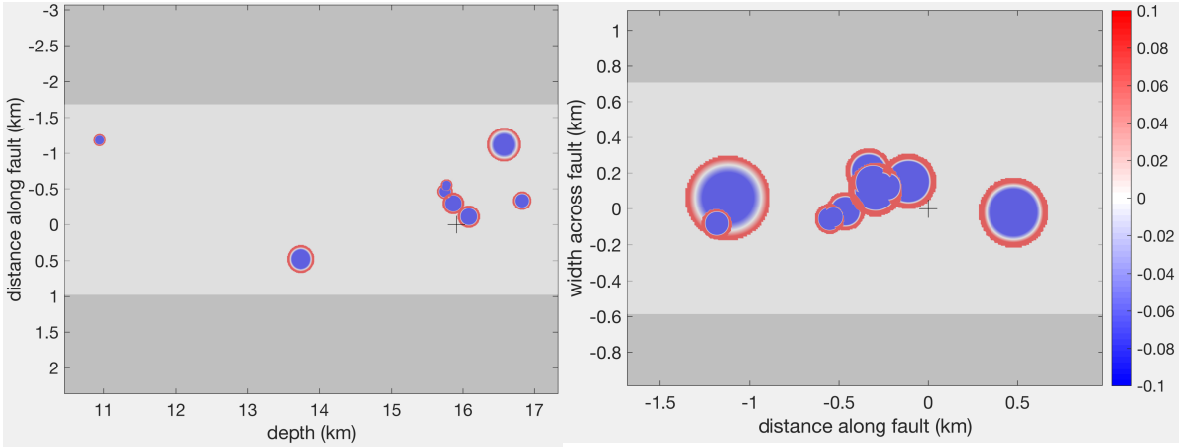

Figure 3. Left: Along-depth view of stress changes. Right: Map view of stress changes. The black "+" indicates the M7.2 mainshock in both figures. Red color is stress increase, and blue is stress decrease. All the following figures use the same colorbar (+/-0.1 MPa).

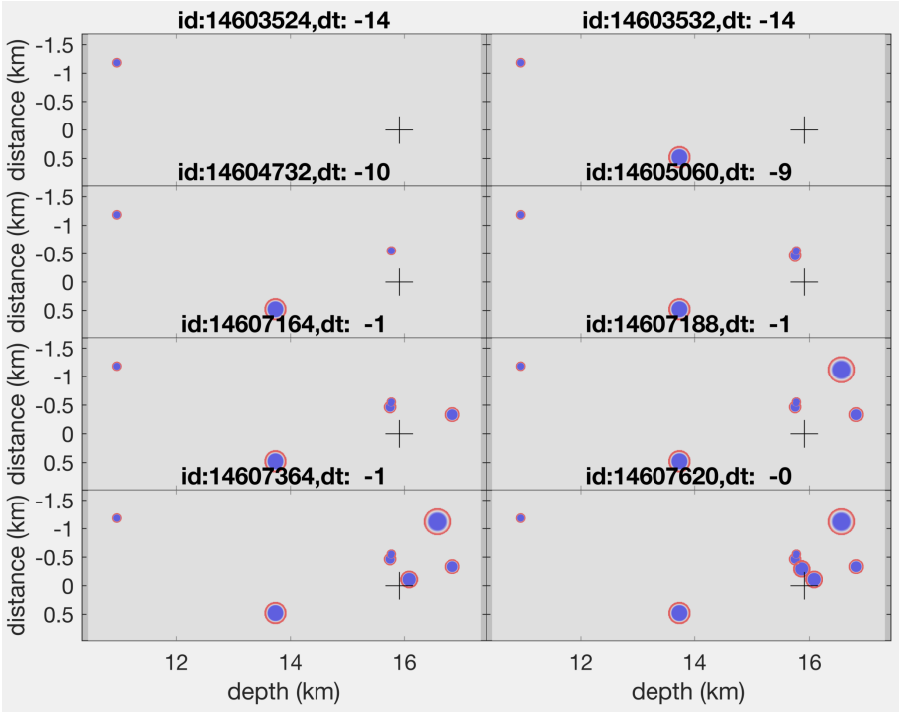

Figure 4. Temporal evolution of stress change from individual foreshocks. Each panel shows cumulative stress change from previous earthquakes. Event ID and days relative to mainshock are shown in the title. Note the clustering of foreshocks near the mainshock during the last day. The black "+" indicates the mainshock.

Conclusion:

In this study, we applied an improved stacking method to new dataset that include stations from Mexico. The new results show good agreement with spectral ratio method using S-wave, suggesting that the new method from Chen & Abercrombie (2020) improves estimation of source parameters.

Figures 3 and 4 are based on relocations from Yao et al., (2020), and the results are similar to P-wave results using SNSS method. However, using the Hauksson et al., (2012) catalog, we only observed stress interactions among foreshock themselves (Figure 5), but no clustering of foreshocks around mainshock hypocenter as shown in Figures 3 and 4.

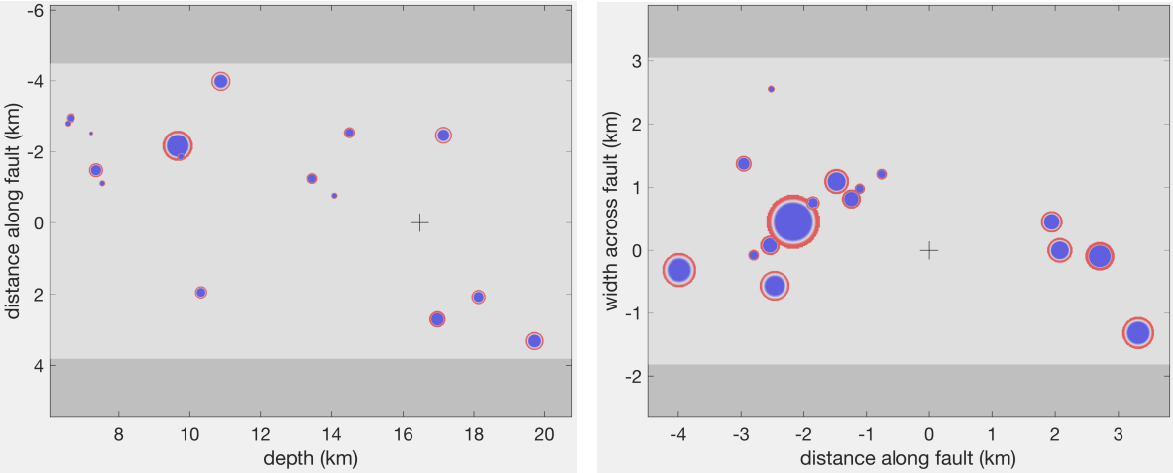

Figure 5. Similar to Figure 3, but using Hauksson et al., (2012) locations. Left: Along-depth view of stress changes. Right: Map view of stress changes. The black "+" indicates the M7.2 mainshock in both figures. No clear triggering relationship between foreshocks and the mainshock is found.

The results suggest that foreshock themselves behave as swarm-like sequences that appear to be independent of mainshock nucleation process. Improved event relocation suggests that some foreshocks can concentrate within several hundred meters from the mainshock hypocenter, and cause stress loading in the mainshock nucleation zone. The mainshock started near the junction of the main NW-oriented fault and the NS-oriented fault with foreshocks. It is possible the foreshocks are continuing to rupture a strong asperity, and eventually lead to runaway rupture that cause the mainshock.

Better understanding of foreshock sequences would require higher-resolution dataset, better earthquake locations, and improved knowledge of source parameters. Comparison between foreshocks and earthquake swarms would help to better understand the triggering relationship between foreshocks and large mainshocks.

Presentations and publications:

We presented preliminary research results at the 2019 annual SCEC meeting: Source characteristics of the foreshock sequence of the 2010 M7.2 El Mayor-Cucapah earthquake: implication for the triggering process, by X. Chen, Q. Wu, D. Yao, & Z. Peng. We plan to reanalyze a few more foreshock sequences, as well as aseismic-slip driven major swarms to compare foreshocks and swarms, and prepare a manuscript detailing the proposed swarmy-foreshock model.

Reference:

Chen, X., & Shearer, P. (2013). California foreshock sequences suggest aseismic triggering process. *Geophys. Res. Lett.*, *40*, 2602–2607. https://doi.org/10.1002/grl.50444

Chen, Xiaowei, & Abercrombie, R. E. (2020). Improved approach for stress drop estimation and its application to an induced earthquake sequence in Oklahoma. *Geophys. J. Int.*, *223*, 233–253. https://doi.org/10.1093/gji/ggaa316

Ellsworth, W. L., & Bulut, F. (2018). Nucleation of the 1999 Izmit earthquake by a triggered cascade of foreshocks. *Nature Geoscience*, (June). https://doi.org/10.1038/s41561-018-0145-1

Eshelby, J. D. (1957). The determination of the elastic field of an ellipsoidal inclusion, and related problems. *Proc. R. Soc. London, Ser. A, 241*, 376–396.

Hauksson, E., Yang, W., & Shearer, P. M. (2012). Waveform Relocated Earthquake Catalog for Southern California (1981 to June 2011). *Bulletin of the Seismological Society of America*, *102*(5), 2239–2244. https://doi.org/10.1785/0120120010

Kaneko, Y., & Shearer, P. M. (2014). Seismic source spectra and estimated stress drop derived from cohesive-zone models for circular subshear rupture. *Geophys. J. Int.* https://doi.org/10.1093/gji/ggu030

Shearer, P. M., Prieto, G. A., & Hauksson, E. (2006). Comprehensive analysis of earthquake spectral in southern California. *Journal of Geophysical Research-Solid Earth*, *111*(B6). https://doi.org/B0630310.1029/2005jb003979

Yao, D., Huang, Y., Peng, Z., & Castro, R. R. (2020). Detailed Investigation of the Foreshock Sequence of the 2010 Mw7.2 El Mayor-Cucapah Earthquake. *Journal of Geophysical Research: Solid Earth*, *125*(6). https://doi.org/10.1029/2019JB019076

Yoon, C. E., Yoshimitsu, N., Ellsworth, W. L., & Beroza, G. C. (2019). Foreshocks and Mainshock Nucleation of the 1999 M w 7.1 Hector Mine, California, Earthquake. *Journal of Geophysical Research: Solid Earth*, *124*(2), 1569–1582. https://doi.org/10.1029/2018JB016383